

# Numerical confirmation of universality of transmission micro-symmetry relations in a four-probe quantum dot

Ming Lei and Hong Guo

*Department of Physics and*

*Centre for the Physics of Materials*

*McGill University*

*Montréal, Québec, H3A 2T8 Canada.*

(October 9, 2018)

## Abstract

We study the crossover behavior of the Hall resistance between the integer quantum Hall regime and a regime dominated by the Aharonov-Bohm oscillations, in a system of 4-probe quantum dot with an artificial impurity confined inside. In a previous study [M. Lei, N.J. Zhu and Hong Guo, Phys. Rev. B. **52**, 16784, (1995)], a peculiar set of symmetry relations between various scattering probabilities were found in this crossover regime. In this paper we examine the universality of this set of symmetry relations using different shapes of the quantum dot and positions of the artificial impurity. The symmetry holds for these changes and we conclude that in this transport regime the general behavior of the Hall resistance is determined by the competition of the quantum Hall and Aharonov-Bohm effects, rather than by the detailed shapes of the structure.

72.20.Dp, 72.10.-d, 73.40.-c, 73.20.Dx

Typeset using REVTEX

## I. INTRODUCTION

Semiconductor nanostructures are unique in offering the possibility of studying quantum transport in an artificial potential landscape. This is the regime of *ballistic transport*, in which scattering with impurities can be neglected and one observes the effect of quantum fluctuations. Indeed, various experiments conducted on such systems observed many interesting phenomena, such as the Aharonov-Bohm (AB) effect [1], quantum Hall effect<sup>1</sup> [2,3], quantum chaotic scattering [4], and bending resistance. The transport properties of a system in this regime can be tailored by varying the geometry of the conductor, in much the same way as one would tailor the transmission properties of an optical waveguide [5]. The formal relation between conduction and transmission, known as the Landauer formula [6–8], has demonstrated its real power in this context. For example, the quantization of the conductance of a quantum point contact [9,10], which is a short and narrow constriction in a two-dimensional (2D) electron gas, can be understood using the Landauer formula as resulting from the discreteness of the number of propagating channels in the constriction. Since in the ballistic transport regime the current limiting factor is provided by the carrier scattering from the structure boundaries, in general the behavior of various resistances sensitively depends on the particular shape of the system.

In mesoscopic physics, one of the important effects is the Aharonov-Bohm effect [1], which illustrates that in a field-free multiply-connected region of space the physical properties of a system depend on the vector potential  $\mathbf{A}$ . It is well understood that Aharonov-Bohm effect is about quantum interference of an one-dimensional electronic system in the presence of a magnetic field. On the other hand, the quantum Hall effect is associated with 2D electronic states in strong magnetic fields. In a semi-classical picture these states correspond to carrier trajectories grazing the sample’s boundary. Quantum mechanically these become the edge states which play an important role in understanding the quantized Hall resistance [11]. In some sample geometries where an effective ring topology is obtained, Aharonov-Bohm type oscillations can be observed in certain ranges of magnetic field while quantum Hall resistance is obtained at stronger fields. A possible example is the case of a disk with a hole threading through the middle. Clearly, when the hole is almost as large as the disk, we have an effectively 1D ring and AB oscillation is anticipated; when the hole is much smaller than the disk and with a strong magnetic field, we recover the annular film sample studied by Halperin [11] where quantized Hall resistance is explained based on the role of edge states. While these limiting cases were well understood and studied, the situation is less clear when the size of the hole or the strength of the magnetic field are such that both the AB and quantum Hall effects are present. It is the purpose of this work to further study this “crossover” transport regime for the cases where the system is connected to the outside by quantum wires forming a scattering junction.

---

<sup>1</sup>In this paper, quantum Hall effect means integer quantum Hall effect.

We focus on studying the Hall resistance of several 4-probe device structures using the Büttiker multi-probe resistance formula [12,13],

$$R_{mn,kl} = \frac{h}{e^2} (T_{km}T_{ln} - T_{kn}T_{lm})/D \quad , \quad (1)$$

where  $T_{mn}$  is the transmission coefficient from probe  $n$  to probe  $m$ , and the factor  $D$  is a subdeterminant of rank three of the matrix formed by the equations for the electric current [12]. Particular structures of interests are shown in Figures (1), (2) and (5). For these systems the Hall resistance is given by  $R_{13,24}$  using Eq. (1). These systems are of the usual Hall-bar structure with an antidot or artificial impurity confined inside at various positions. Experimentally these structures can be fabricated by the recently developed multilevel fabrication technique [14], and very interesting anomalous transmission behavior has already been observed in a 2-probe situation [15]. Clearly, when the magnetic field is high, *e.g.*,  $l_s/l_B \gg 1$  with  $l_s$  the “constriction length” (see Fig. (1)) and  $l_B = \sqrt{\hbar c/eB}$  the “magnetic length”, quantum Hall regime is reached. In this case each perfectly transmitting channel or edge state contributes a factor of  $e^2/h$  to the Hall conductance, thus  $N$  such channels give rise to a quantized conductance  $G = N\frac{e^2}{h}$ . On the other hand, if the size of the antidot is so large such that  $l_s/l_B \ll 1$ , the structure is effectively a ring since the conducting electrons do not probe the corners of the quantum dot very much. In this case we expect to and indeed observe AB oscillations [16]. However when the length scales are such that  $l_s/l_B \sim 1$ , we enter the crossover regime and the transmission properties become complicated.

In a previous paper [16], we have made an investigation of this crossover regime using the device structure of Fig. (1). There, we have systematically varied the radius of the antidot and the strength of the magnetic field  $B$ . We have found that for a range of these parameters the transport behavior enters a peculiar regime where a very interesting “micro-symmetry” (see below) exists between various transmission probabilities. The consequence of this symmetry was the observation of an anomalous Hall plateau before the quantum Hall regime is reached, namely an Hall plateau was observed without the establishment of perfectly transmitting edge states. Furthermore, we found that this set of symmetry relations could be explained based on the general topological equivalence of the dominating transmission patterns [12]. Clearly, a further and important question to ask is whether or not this set of peculiar symmetry relations hold for other shapes of the scattering junction (such as for that of Fig. (2)), or for systems without an obvious 4-fold rotational symmetry (such as for those in Fig. (5)). Since the topological equivalence argument which “derives” the micro-symmetry relations [16] is quite general and does not depend on system details, we expect an “universal” behavior of the scattering probability. Namely, the symmetry relations observed in the system of Fig. (1) should also manifest in other systems shown in Figs. (2) and (5). Indeed this is what is obtained from our numerical study to be presented below. Thus we may conclude that the micro-symmetry relations obtained in Ref. [16] is general, and is an universal behavior of this peculiar crossover transport regime.

The paper is organized as the following. In the next section, for completeness and ease

of discussion, we briefly summarize the findings of our earlier work of Ref. [16]. Section III present our investigation of the universality of the symmetry relations. Finally a summary and discussion is presented in the last section.

## II. THE MICRO-SYMMETRY

In order to make the presentation clearer, in this section we briefly review the micro-symmetry relationships we have found in a previous study for the quantum dot system shown in Fig. (1). The details have been included in Ref. [16] and interested readers should refer to that article for complete results.

Consider this structure with the quantum dot size  $D = 2W$  where  $W$  is the width of the probes, taken to be  $1650\text{\AA}$ . For an incoming electron energy  $kW = 9.5$  which is just above the third subband energy when magnetic field is absent, let's make sure that there are at least two transmitting channels through the system for even the largest antidot radius  $r_a$  which we study. We have found, as mentioned in the Introduction, that for small  $r_a$  one obtained a quantized Hall resistance when  $B$  is such that perfectly transmitting edge states are established from probe I to II. On the other hand for a very large  $r_a$ , one observed typical AB oscillations. For an intermediate range of  $r_a$  with a given value of  $B$ , the crossover regime is reached and Ref. [16] has shown the following concerning this crossover regime:

- (1). If we denote  $T_{ij,mn}$  as the probability of an electron incoming from probe  $n$  at channel  $j$ , and going into probe  $m$  at channel  $i$ , then Ref. [16] shows that the following “micro-symmetry” hold approximately

$$\begin{aligned} T_{11,11} &= T_{22,21} & T_{22,11} &= T_{11,21} , \\ T_{21,11} &= T_{12,21} & T_{12,11} &= T_{21,21} , \\ T_{11,31} &= T_{22,41} & T_{22,31} &= T_{11,41} , \\ T_{21,31} &= T_{12,41} , & T_{12,31} &= T_{21,41} . \end{aligned} \quad (2)$$

These symmetry relations are nontrivial. In Ref. [16] we have “derived” these relations using a topological equivalence argument based on the dominating transmission patterns.

- (2). Because of this micro-symmetry (2), we easily deduce the following relations between transmission coefficients of individual channels:

$$T_{11}^1 = T_{21}^2 , \quad T_{21}^1 = T_{11}^2 , \quad T_{31}^1 = T_{41}^2 , \quad T_{41}^1 = T_{31}^2 , \quad (3)$$

which indicate that the reflection coefficient of channel 1,  $T_{11}^1$ , equals the transmission coefficient to probe II of channel 2,  $T_{21}^2$ ; and that the transmission coefficient to probe III of channel 1,  $T_{31}^1$ , equals the transmission coefficient to probe IV of channel 2,  $T_{41}^2$ .

(3). Moreover, for the structure of Fig. (1) the transmission coefficients happen [16] to approximately have the following values in the crossover regime:

$$\begin{aligned}
T_{11} &\equiv T_{11}^1 + T_{11}^2 = 1, \\
T_{21} &\equiv T_{21}^1 + T_{21}^2 = 1, \\
T_{31} &\equiv T_{31}^1 + T_{31}^2 = 0, \\
T_{41} &\equiv T_{41}^1 + T_{41}^2 = 0.
\end{aligned} \tag{4}$$

Obviously we expect that these particular values are system dependent.

(4). One consequence of the symmetry relations (2) and (3) is, using the Büttiker formula, that Hall resistance  $R_H$  takes an apparent plateau (quantized) value before perfectly transmitting edge states are established. With the particular values of the transmission coefficients which are given by (4), this abnormal Hall plateau has the value of  $1 \times \frac{h}{e^2}$ .

### III. UNIVERSALITY OF THE MICRO-SYMMETRY

In this section, we investigate the universality of the micro-symmetry in the crossover regime which is summarized in the last section. Our main task is to answer the following question: is the micro-symmetry a universal property of the crossover transport regime without or with only weak dependence on the particular geometric shape of the sample ? Although the topological equivalence argument [16] seems to give a positive answer to this question, we are not aware of any analytical technique which can give a rigorous derivation of this micro-symmetry. The difficulty comes from the fact that a complicated 2D scattering problem must be solved in order to obtain the various transmission probabilities. Hence we have decided to numerically examine several different systems and numerically compute the scattering probabilities to check the validity of the symmetry relations presented in the last section. We emphasize that this work is a numerical establishment of the generic behavior of the crossover regime, rather than a rigorous proof.

The quantum scattering problem is solved using the finite-element numerical scheme of Ref. [17,18]. Essentially we discretize the scattering region which is the quantum dot into a fine grid of finite elements. This procedure reduces the solution of the Schrödinger equation into a sparse matrix problem. The quantum propagation in the probes is solved separately using the method outlined in Ref. [19]. The wavefunctions and their spatial derivatives are matched at the probe boundaries, and this leads to the transmission probabilities and coefficients. We have checked, for all the systems studied below, that numerical convergence is obtained using around 5000 grid points. As shown in our earlier work [16] and discussed

above, the crossover transport regime is reached for a range of appropriate values of the anti-dot size  $r_a$  and the magnetic field  $B$ . To save computation requirement in this work we have fixed  $B$  at a reasonablely large value and varied the size  $r_a$  to reach the crossover regime.

### A. Circular quantum dot

First, let's consider the situation where the geometry shape of the quantum dot is changed to circular, see Fig. (2). The antidot is still fixed at the center of the (circular) quantum dot. The parameters  $W$ ,  $D$  and  $kW$  are the same as those used in Ref. [16] and quoted in the last section. To investigate the crossover regime, we fix the magnetic field  $B$  at 6060 Gauss and vary the antidot radius  $r_a$ . At this value of  $B$ , only the first two quantum channels in the probes can propagate.

Fig (3) shows the transmission coefficient  $T_{m1}$ , ( $m = 1, 2, 3, 4$ ) and Hall resistance  $R_H$  as a function of antidot radius  $r_a$ . Here  $T_{m1}$  is the total transmission coefficient from probe I to probe  $m$  including all the two propagating channels. From Fig. (3a) we can find that there is a regime with intermediate values of  $r_a$ :  $0.45W < r_a < 0.60W$ , where the relations of Eq. (4) indeed roughly hold. Thus, just as what happened for the structure of Fig. (1), using the Büttiker formula we arrive at the abnormal Hall plateau  $R_H \approx 1 \times h/e^2$  for this range of  $r_a$ , where both propagating channels are only partially transmitting. Furthermore, inspecting Fig. (4) which plots the transmission coefficients of individual propagating channels, we see that relations of Eq. (3) are also approximately satisfied. Here since  $T_{31}^i$  and  $T_{41}^i$  are almost zero in the crossover regime, they are not shown in Fig. (4).

To test the micro-symmetry relations Eq. (2) for the present structure, in Table (1) various transmission probabilities are tabulated for a given magnetic field  $B = 6060$  Gauss for several values of the antidot radius  $r_a$ . Clearly our numerical data are consistent with Eqs. (2), which are supported by the general topological equivalence argument [16]. We recall that the equal signs in Eqs. (2) are only rigorously satisfied by the limiting cases of perfectly transmitting or reflecting transport channels, as shown in our earlier work [16]. In this sense the consistency of our data in Table (1) with Eq. (2) is quite respectable. Thus we may conclude that in the crossover regime of the structure shown in Fig. (2), our topological argument and the micro-symmetry still approximately hold, and these features do not depend strongly on the shapes of the Hall junction, at least as far as the kind of changes to the Hall junction we have made here, and an abnormal Hall plateau can still be observed due to these features.

On the other hand, there are several features which do depend on the details of the scattering junction, as shown in Figs. (3) and (4). First, for a small antidot *e.g.*  $0 < r_a < 0.45W$  and at this field  $B = 6060$  Gauss, we don't have two perfect transmission channels as what was found [16] for the structure of Fig. (1). *i.e.*, instead of  $T_{21} = 2$  and  $T_{11} = 0$ , we now have  $T_{21} \approx 1.05$ ,  $T_{11} \approx 0.77$ ,  $T_{31} \approx 0.15$ , and  $T_{41} \approx 0.03$ . Second, the transition from the

crossover regime to the regime dominated by AB oscillations (large antidot) is much sharper here. Finally, the circular-shaped quantum dot gives rise to relatively more Hall resistance fluctuations than that of the square-shaped quantum dot studied before [16]. However these features which depend on the particular shapes of the scattering junction, are all related to the values of transmission coefficients, which, as was well understood in the literature, are expected to be sensitive to details of the scattering.

The above numerical results approximately confirms that the appearance of crossover regime and the correctness of Eqs. (2), (3) and (4) are quite universal in the sense that they do not depend strongly on the particular quantum dot structure we choose. Furthermore, our topological explanation of the micro-symmetry in the crossover regime [16] does not rely on the exact position where the antidot is positioned. Nevertheless so far the structures studied all had the antidot positioned at the center of the quantum dot making the systems 4-fold rotational symmetric. Hence to further establish the transport universality of the crossover regime, in the following we investigate situations where the antidot is located away from the center.

## B. Asymmetric junction

Consider the Hall junction illustrated in Fig. (5a). All system parameters are the same as before except that the center of the antidot is now located at the position  $(-W/10, -W/10)$  (assuming the center of the whole structure is at  $(0,0)$ ). The magnetic field is fixed at  $B = 6060$  Gauss which belongs to the crossover regime field strength.

Our numerical calculation seems to provide a positive answer to the question of universality. Fig. (6a1) shows the transmission coefficient  $T_{m1}$ , ( $m = 1, 2, 3, 4$ ) which unambiguously demonstrates that Eq. (4) still holds here. To test micro-symmetry relations and topological explanation of Ref. [16], Fig. (6a2) and Table (2a) show that Eqs. (3) and (2) are indeed satisfied.

Since the center of the antidot is a 4-fold symmetric point inside the quantum dot, we need to calculate the transmission coefficients of all the other three cases (Fig. (5b,5c,5d)) in order to compute the Hall resistance  $R_H$  using the Büttiker formula Eq. (1). Obviously the micro-symmetry relations of the crossover regime should hold for all these situations. Indeed, Figs. (6b,6c,6d) and Tables (2b,2c,2d) confirm that Eqs. (4), (3) and (2) are satisfied for all the cases. Hence the generic behavior of the crossover regime has no dependence on the position of the antidot.

Now let us calculate the Hall resistance  $R_H$  for the structure of Fig. (5a) when electrons are incoming from probe I. Making use of the spatial topological symmetry of the four structures in Fig. (5), the transmission probabilities with electrons coming from probes other than probe I of one structure can be obtained by a permutation of the transmission probabilities with electrons coming from probe I of other structures. In particular, for the transmission coefficients we find

$$T_{mn}^{(\alpha)} = T_{m+5-n,1}^{(\alpha+5-n)}, \quad (m,n = 1,2,3,4; \alpha = a,b,c,d) , \quad (5)$$

where  $T_{mn}^{(\alpha)}$  is the transmission coefficient from probe  $n$  to probe  $m$  of structure  $\alpha$  in Fig. (5) and where the index of  $T_{mn}^{(\alpha)}$  is taken to be modulo 4. For the sake of discussion we employ another form of Büttiker formula (equivalent to Eq. (1)) [8],

$$R_{mn,kl} = \frac{\alpha_{21}}{\alpha_{11}\alpha_{22} - \alpha_{12}\alpha_{21}} , \quad (6)$$

where

$$\alpha_{11} = \frac{e^2}{h}[(N - T_{mm})S - (T_{ml} + T_{mk})(T_{lm} + T_{km})]/S , \quad (7)$$

$$\alpha_{12} = \frac{e^2}{h}[T_{mk}T_{nl} - T_{ml}T_{nk}]/S , \quad (8)$$

$$\alpha_{21} = \frac{e^2}{h}[T_{km}T_{ln} - T_{lm}T_{kn}]/S , \quad (9)$$

$$\alpha_{22} = \frac{e^2}{h}[(N - T_{kk})S - (T_{km} + T_{kn})(T_{nk} + T_{mk})]/S , \quad (10)$$

and

$$S = T_{mk} + T_{ml} + T_{nk} + T_{nl} = T_{km} + T_{lm} + T_{kn} + T_{ln} . \quad (11)$$

Here  $N$  is the number of quantum channel occupied by the incident electron, in our case  $N = 2$ .

Fig. (7) shows the dependence of Hall resistance  $R_H$  on the radius  $r_a$  of the antidot corresponding to the four Hall-bar structures of Fig. (5), respectively. It is obvious that the peculiar crossover regime still exists in every situation, signaled by the appearance of a Hall “plateau” as  $r_a$  is increased into the crossover regime. We emphasize that this abnormal plateau is not due to the establishment of perfectly transmitting edge states when quantum Hall regime is reached. They are due to the micro-symmetry properties of the crossover regime. Hence within the scope of our investigations these properties are universal against the changes of the antidot position.

Inspecting Fig. (7) carefully, we find that the behavior of Hall resistance of structure (a) and (c) are quite similar, and so are the ones of structures (b) and (d). Since structures (a) and (c), (b) and (d) are spatial reversal symmetric, it seems that an interesting property is obtained,

$$R_H(\mathbf{r}) \approx R_H(-\mathbf{r}) , \quad (12)$$

where  $\mathbf{r}$  is the position of the center of the antidot.

In fact, this interesting feature is a natural result of the permutation relation Eq. (5) and the Büttiker formula Eq. (6). With the help of Eqs. (5)–(11), it is rather straight forward to obtain the following relations

$$S^{(a)} = S^{(c)}, \quad \alpha_{12}^{(a)} = \alpha_{12}^{(c)}, \quad \alpha_{21}^{(a)} = \alpha_{21}^{(c)}, \quad (13)$$

$$S^{(b)} = S^{(d)}, \quad \alpha_{12}^{(b)} = \alpha_{12}^{(d)}, \quad \alpha_{21}^{(b)} = \alpha_{21}^{(d)}. \quad (14)$$

Here the superscripts  $(a, b, c, d)$  indicate the structures of Fig. (5), *i.e.*  $\alpha_{12}^{(a)}$  is the  $\alpha_{12}$  for structure of Fig. (5a). Furthermore, we notice that except two transition regimes (one is from small-antidot regime to crossover regime and the other is from crossover regime to large-antidot regime), the behavior of transmission coefficients of structures (a) and (d) are much alike and so are those of structures (b) and (c), *i.e.*,

$$T_{m1}^{(a)} \approx T_{m1}^{(d)}, \quad T_{m1}^{(b)} \approx T_{m1}^{(c)}, \quad (m = 1, 2, 3, 4). \quad (15)$$

Consequently we find

$$\alpha_{11}^{(a)} \alpha_{22}^{(a)} \approx \alpha_{11}^{(c)} \alpha_{22}^{(c)}, \quad (16)$$

$$\alpha_{11}^{(b)} \alpha_{22}^{(b)} \approx \alpha_{11}^{(d)} \alpha_{22}^{(d)}. \quad (17)$$

Based on Eqs. (14)–(17), it is trivial to obtain the center-reversal property of  $R_H$  (eq. (12)).

#### IV. SUMMARY

In this work we have studied the universality of the micro-symmetry of transmission coefficients for the peculiar crossover transport regime established when both quantum Hall and AB effects compete. This crossover regime is reached when the antidot radius is increased. For a square quantum dot with the antidot located in the center, the crossover regime is marked by the appearance of a host of non-trivial symmetries between various transmission probabilities. The consequence of this set of symmetries is the observation of an abnormal Hall plateau before the true quantum Hall regime is reached. We have established the universality of this micro-symmetry from two directions. First, it is confirmed numerically that for a circular Hall junction there is also a crossover regime as the antidot size is increased where the micro-symmetry of transmission probabilities approximately holds. Second, when the 4-fold rotational symmetry is broken by shifting the antidot positions, the same crossover behavior is obtained. Since, as we have shown in Ref. [16], that the micro-symmetry relations are supported by the topological equivalence argument of Büttiker [12], our numerical calculations presented here give further confirmation of that argument. We may thus conclude that the behavior of the crossover transport regime, namely the set of micro-symmetry relations, are generic and robust against the change of shapes of the scattering junction.

Finally we wish to emphasize that the universality of the crossover behavior is established here from a *numerical “experiment”*. Hence it will be useful but very challenging to analytically derive the formula for transmission coefficients in order to definitely prove the micro-symmetry relations. Furthermore, our numerical calculations were carried out for system parameters such that only two propagating channels are possible, which is the simplest case where the topological equivalent argument could be applied [16]. If there are more propagating channels, the micro-symmetry relations may become more complicated and more interesting.

## **V. ACKNOWLEDGMENTS**

We thank Ningjia Zhu and Haiqing Wei for many useful discussions. We gratefully acknowledge support from the Natural Sciences and Engineering Research Council of Canada, and le Fonds pour la Formation de Chercheurs et l’Aide à la Recherche de la Province du Québec.

## REFERENCES

- [1] Y. Aharonov and D. Bohm, Phys. Rev. **115**, 485 (1959).
- [2] K. von Klitzing and G. Dorda and M. Pepper, Phys. Rev. Lett. **45**, 495 (1980).
- [3] K. von Klitzing, Rev. of Mod. Phys, **58**, 519 (1986).
- [4] C.M. Marcus, A.J. Rimberg, R.M. Westervelt, P.F. Hopkins and A.C. Gossard, Phys. Rev. Lett. **69**, 506 (1992).
- [5] H. van Houten and C. W. J. Beenakker, *Analogies in Optics and Microelectronics*, edited by W. Van Haeringen and D. Lenstra, Kluwer Academic Press, Dordrecht 1990.
- [6] Y. Imry, *Directions in Condensed Matter Physics*, edited by G. Grinstein and G. Mazenko, World Scientific Press, Singapore 1986.
- [7] R. Landauer, IBM Res. Dev, **1**, 223, (1957).
- [8] M. Büttiker, Phys. Rev. Lett. **57** 1761 (1986).
- [9] B. J. van Wees and H. Van Houten and C. W. J. Beenakker and J. G. Williamson and L. P. Kouwenhoven and D. van der Marel and C. T. Foxon, Phys. Rev. Lett. **60**, 848 (1988).
- [10] D. A. Wharam and T. J. Thornton and R. Newbury and M. Pepper and H. Ahmed and J. E. F. Frost and D. G. Hasko and D. A. Ritchie and G. A. C. Jones, J. Appl. Phys. **61**, 4723 (1987).
- [11] B.I. Halperin, Phys. Rev. B. **25**, 2185 (1982).
- [12] M. Büttiker, Phys. Rev. B. **38**, 12724 (1988).
- [13] M. Büttiker, IBM J. Res. Dev. **32**, 317 (1988); Phys. Rev. Lett. **62**, 229 (1989).
- [14] Y. Feng, *et. al.*, Appl. Phys. Lett., **63**, 3191 (1993).
- [15] G. Kirczenow, *et. al.*, Phys. Rev. Lett. **72**, 2069 (1994).
- [16] M. Lei, N.J. Zhu and H. Guo, Phys. Rev. B. **52**, 16784, (1995).
- [17] C.S. Lent, Appl. Phys. Lett. **67**, 6353 (1990).
- [18] Yongjiang Wang, Jian Wang and Hong Guo, Phys. Rev. B. **49**, 1928 (1994).
- [19] R.L. Schult, H.W. Wyld, and D.G. Ravenhall, Phys. Rev. B. **38**, 12760 (1990).

## FIGURES

FIG. 1. Schematic plot of the Hall junction studied in Ref. [16]. An antidot of radius  $r_a$  is confined inside the square quantum dot and positioned at the center. Electrons incident from probe I.

FIG. 2. Schematic plot of a circular Hall junction. An antidot of radius  $r_a$  is confined inside the junction at the center. Electrons incident from probe I.

FIG. 3. (a) Transmission coefficients  $T_{mn}$  of the circular junction in Fig. (2) as a function of the antidot radius  $r_a$  at  $B = 6060$  Gauss. Note in the crossover regime  $T_{11} \approx T_{21} \approx 1$  while  $T_{31} \approx T_{41} \approx 0$ . Solid line is  $T_{11}$ , dashed line is  $T_{21}$ , short-dashed line is  $T_{31}$  and dot-dashed line is  $T_{41}$ . (b) Hall resistance  $R_H$  as a function of  $r_a$  at  $B = 6060$  Gauss. The crossover regime is marked by the abnormal Hall “plateau”  $\sim h/e^2$ .

FIG. 4. Transmission coefficients of the circular Hall junction for individual incoming channels  $T_{mn}^i$ , where  $i$  is the channel number, as a function of  $r_a$  at  $B = 6060$  Gauss. Note in the crossover regime  $T_{11}^1 \approx T_{21}^2$ ,  $T_{21}^1 \approx T_{11}^2$ . Solid line is  $T_{11}^1$ , dashed line is  $T_{21}^1$ , short-dashed line is  $T_{21}^2$  and dot-dashed line is  $T_{11}^2$ .

FIG. 5. Schematic plot of the Hall junctions with the antidot away from the center. Electrons incident from probe I. The centers of the antidots of structure (a), (b), (c) and (d) are located at positions  $(-W/2, -W/2)$ ,  $(W/2, -W/2)$ ,  $(W/2, W/2)$  and  $(-W/2, W/2)$  respectively.  $W$  is the width of the probes and point  $(0,0)$  is the center of the Hall junctions.

FIG. 6. Transmission coefficients of the structure shown in Fig. (5a,5b,5c,5d). (a1,b1,c1,d1): Transmission coefficients  $T_{mn}$  as a function of  $r_a$  at  $B = 6060$  Gauss. Note that in the crossover regime  $T_{11} = T_{21} = 1$  while  $T_{31} = T_{41} = 0$ . Solid line is  $T_{11}$ , dashed line is  $T_{21}$ , short-dashed line is  $T_{31}$  and dot-dashed line is  $T_{41}$ . (a2,b2,c2,d2): Transmission coefficients of individual incoming channels  $T_{mn}^i$  as a function of  $r_a$  at  $B = 6060$  Gauss. Note in the crossover regime  $T_{11}^1 = T_{21}^2$ ,  $T_{21}^1 = T_{11}^2$ . Solid line is  $T_{11}^1$ , dashed line is  $T_{21}^1$ , short-dashed line is  $T_{21}^2$  and dot-dashed line is  $T_{11}^2$ .

FIG. 7. Hall resistance  $R_H$  for the four structures in Fig. (5) as a function of  $r_a$  at  $B = 6060$  Gauss. The crossover regime is marked by the abnormal Hall “plateau” of  $\sim h/e^2$ . (a), (b), (c) and (d) are for the junctions Fig. (5a, 5b, 5c and 5d) respectively.

Table (1). Transmission coefficients  $T_{ij,mn}$  of the circular-shaped Hall junction for different antidot size  $r_a$  at  $B = 6060$  Gauss. The data shows approximately the micro-symmetry of Eq. (2).

$T_{ij,mn}$	$B = 6060$ Gauss			
	$r_a=0.45W$	$r_a=0.50W$	$r_a=0.55W$	$r_a=0.60W$
$T_{11,11}$	0.19625	0.16980	0.16338	0.15926
$T_{22,21}$	0.15906	0.14777	0.13730	0.14367
$T_{22,11}$	0.35758	0.38569	0.39566	0.39751
$T_{11,21}$	0.36527	0.37547	0.37030	0.36799
$T_{21,11}$	0.22735	0.22241	0.22440	0.23028
$T_{12,21}$	0.25799	0.24585	0.24189	0.22988
$T_{12,11}$	0.22701	0.22224	0.22432	0.22024
$T_{21,21}$	0.19286	0.21024	0.23071	0.24458

Table (2). Transmission coefficients  $T_{ij,mn}$  of square-shaped Hall junction for different antidot size  $r_a$  at  $B = 6060$  Gauss. The data shows approximately the micro-symmetry of Eq. (2). The four tables labeled (a)–(d) correspond to the four cases of Fig. (5).

(a)		$B = 6060$ Gauss			
		$r_a=0.45W$	$r_a=0.50W$	$r_a=0.55W$	$r_a=0.60W$
$T_{11,11}$		0.05562	0.04323	0.05066	0.02705
$T_{22,21}$		0.06449	0.05176	0.11119	0.02531
$T_{22,11}$		0.51773	0.57690	0.50621	0.74003
$T_{11,21}$		0.50523	0.58387	0.51868	0.70998
$T_{21,11}$		0.22367	0.20044	0.27021	0.14702
$T_{12,21}$		0.20345	0.18064	0.17242	0.13588
$T_{12,11}$		0.18651	0.17520	0.17257	0.08857
$T_{21,21}$		0.22118	0.17618	0.15352	0.11026

(b)		$B = 6060$ Gauss			
		$r_a=0.50W$	$r_a=0.55W$	$r_a=0.60W$	$r_a=0.65W$
$T_{11,11}$		0.07671	0.08561	0.05593	0.03802
$T_{22,21}$		0.06021	0.04987	0.02631	0.01327
$T_{22,11}$		0.42673	0.46831	0.54855	0.61120
$T_{11,21}$		0.50997	0.50551	0.59186	0.64374
$T_{21,11}$		0.21832	0.27954	0.22030	0.17901
$T_{12,21}$		0.22536	0.26623	0.23354	0.18041
$T_{12,11}$		0.17649	0.16623	0.17363	0.16191
$T_{21,21}$		0.16720	0.13305	0.13545	0.11159

(c)		$B = 6060Gauss$			
		$r_a=0.60W$	$r_a=0.625W$	$r_a=0.65W$	$r_a=0.675W$
$T_{11,11}$		0.05560	0.07254	0.03809	0.04321
$T_{22,21}$		0.07046	0.09014	0.04203	0.03209
$T_{22,11}$		0.51735	0.46176	0.61005	0.61994
$T_{11,21}$		0.51742	0.45744	0.61337	0.65171
$T_{21,11}$		0.21657	0.22544	0.16602	0.14622
$T_{12,21}$		0.18755	0.19846	0.15711	0.15401
$T_{12,11}$		0.20810	0.23056	0.17426	0.18120
$T_{21,21}$		0.21923	0.25808	0.18054	0.14963

(d)		$B = 6060Gauss$			
		$r_a=0.45W$	$r_a=0.50W$	$r_a=0.55W$	$r_a=0.60W$
$T_{11,11}$		0.05564	0.04329	0.05162	0.02766
$T_{22,21}$		0.06345	0.06690	0.07459	0.02671
$T_{22,11}$		0.51416	0.51615	0.48591	0.73881
$T_{11,21}$		0.49947	0.48176	0.46726	0.68993
$T_{21,11}$		0.20006	0.18348	0.17073	0.08608
$T_{12,21}$		0.19157	0.15113	0.14174	0.07760
$T_{12,11}$		0.21018	0.25320	0.28065	0.19681
$T_{21,21}$		0.24069	0.29544	0.30648	0.24394

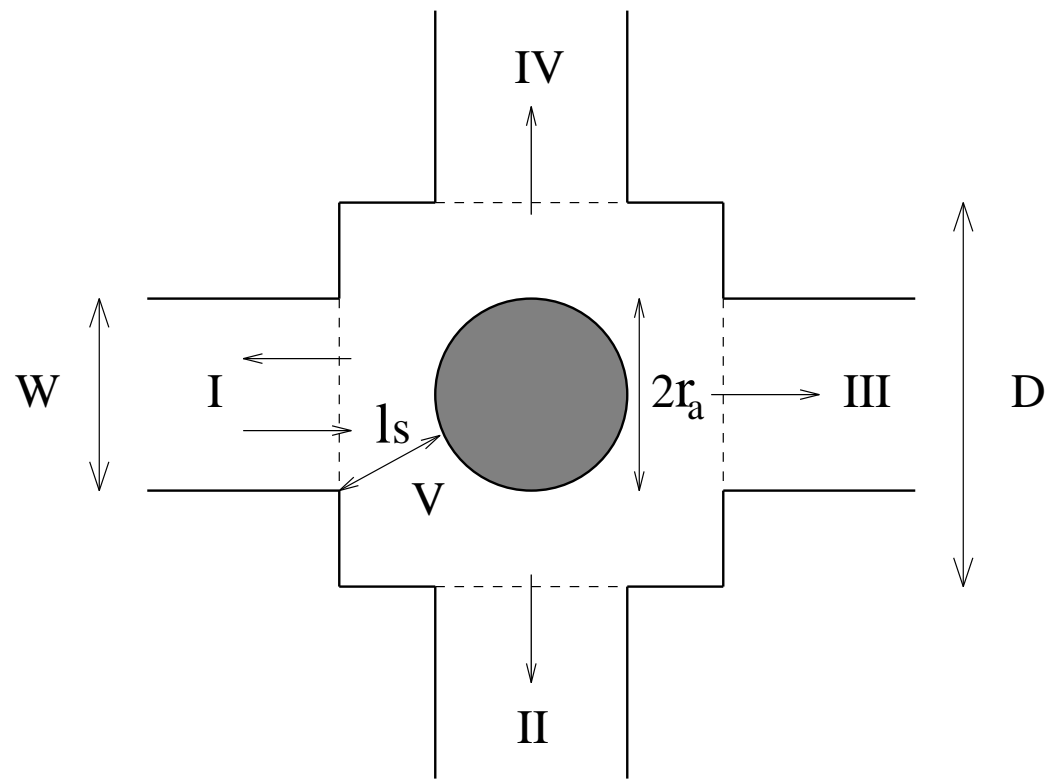


**Fig. 1**

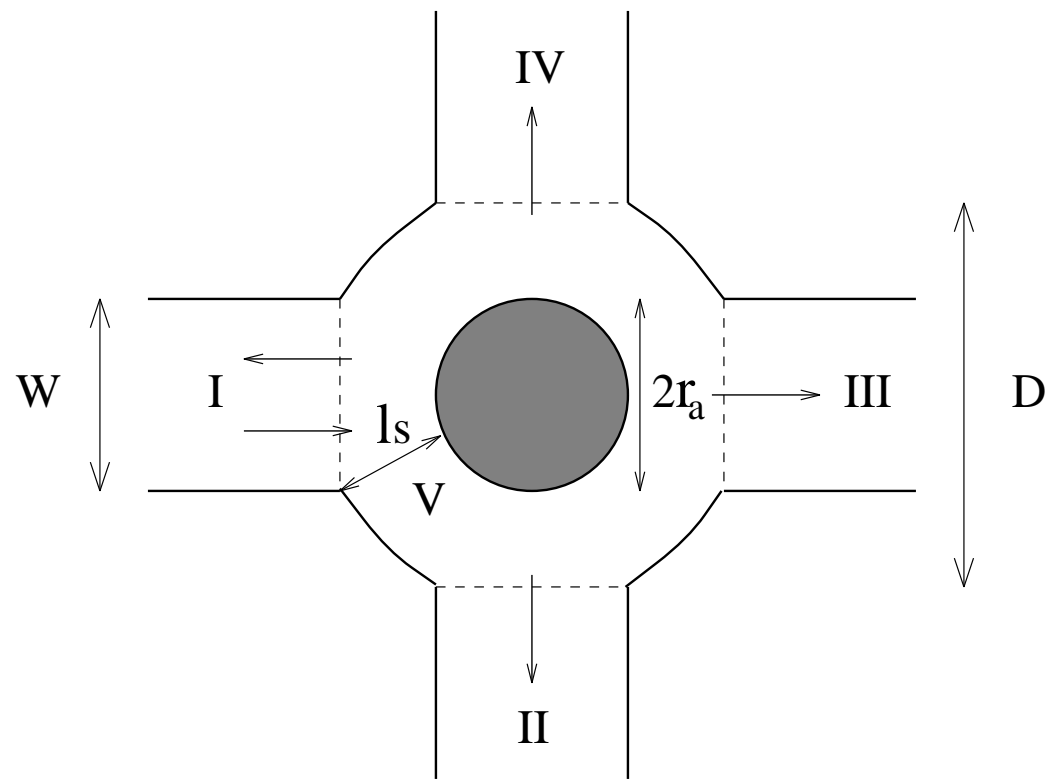


**Fig. 2**

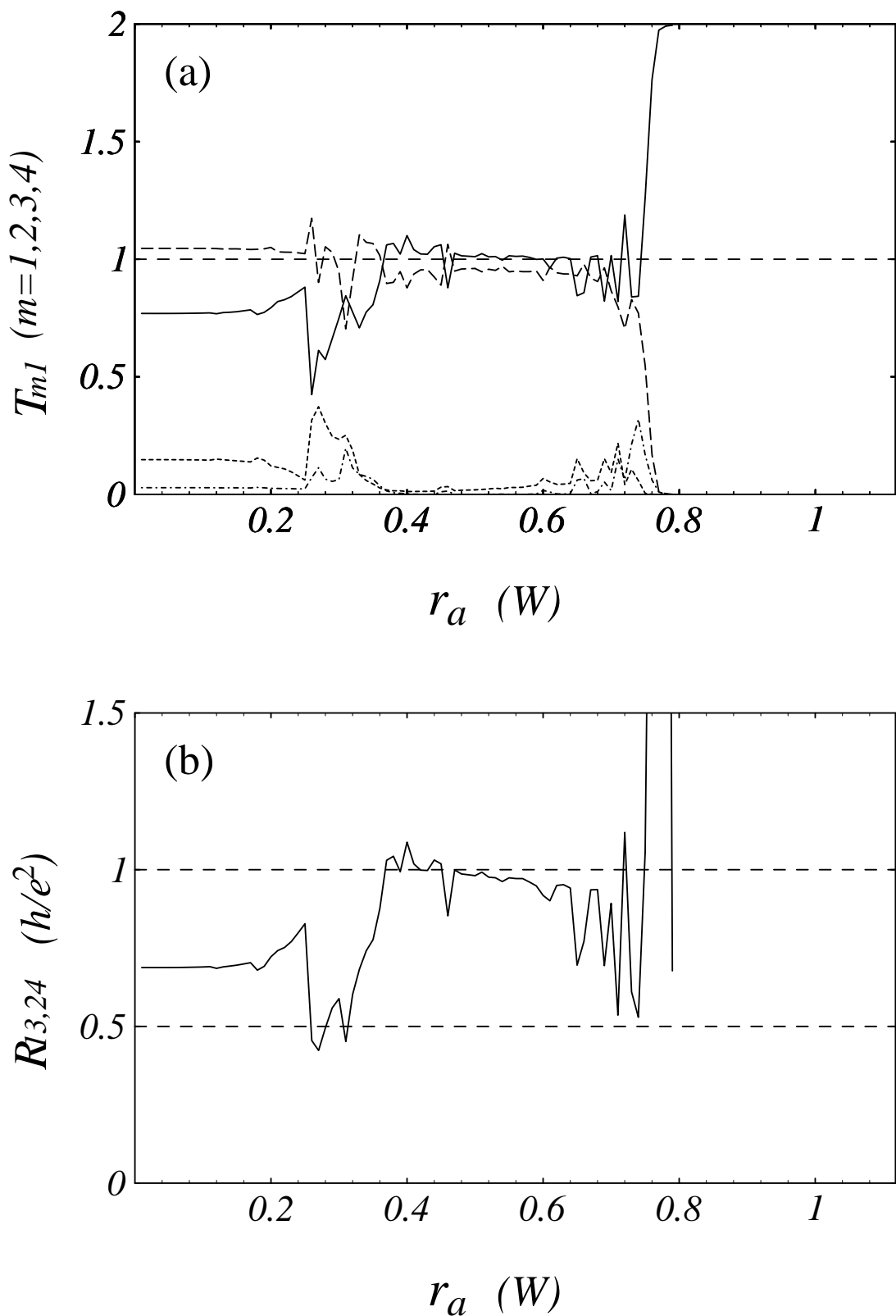


**Fig. 3**

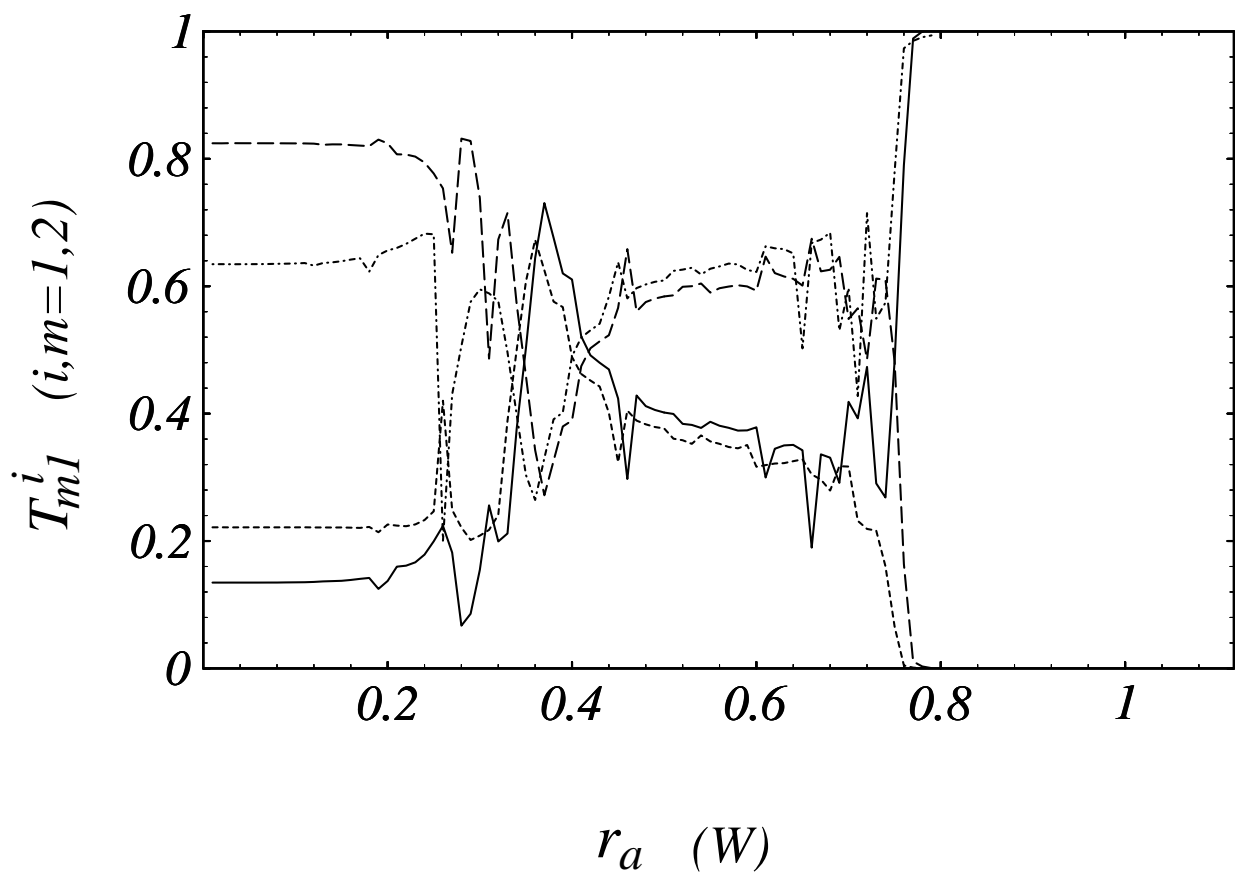
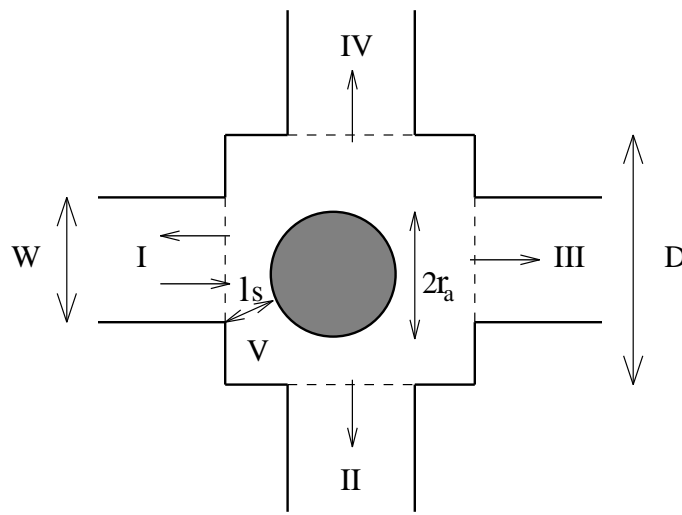
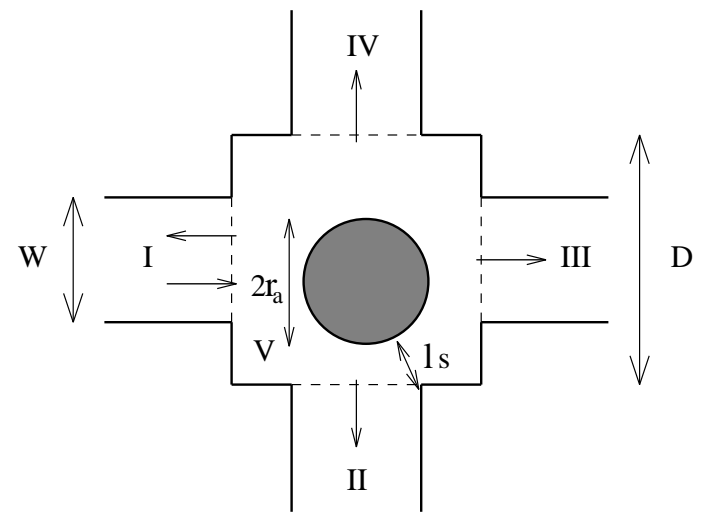


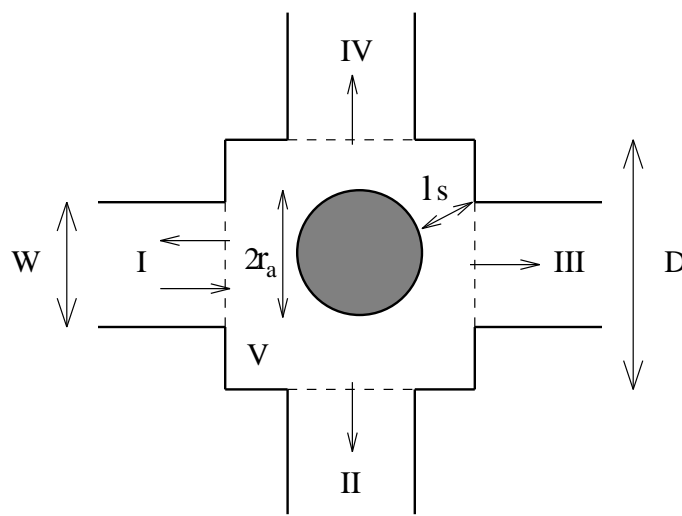
**Fig. 4**



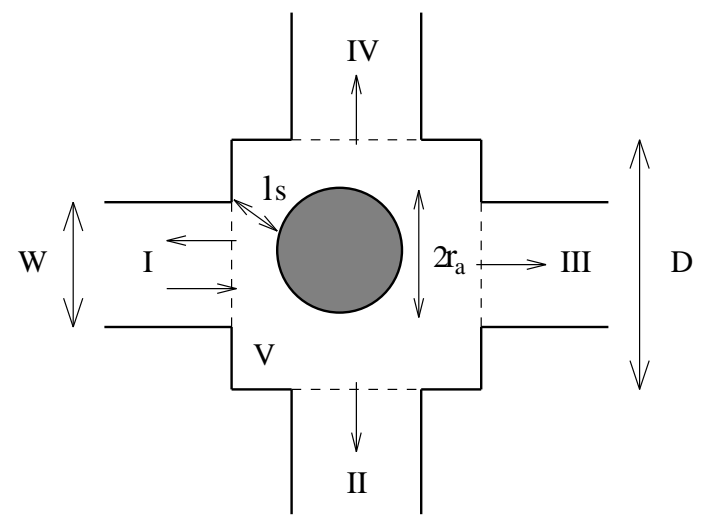
(a)



(b)

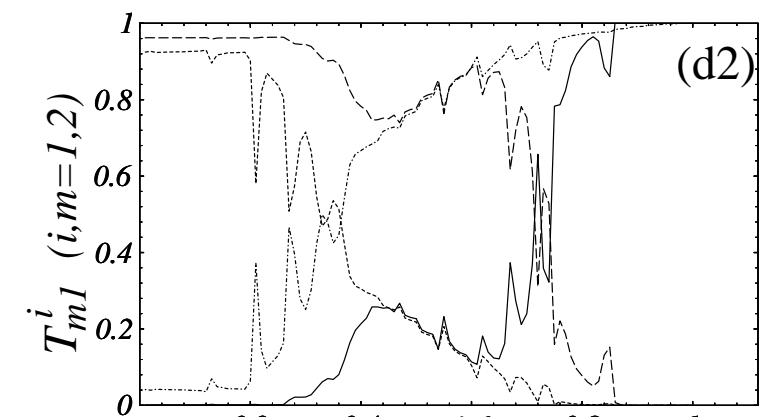
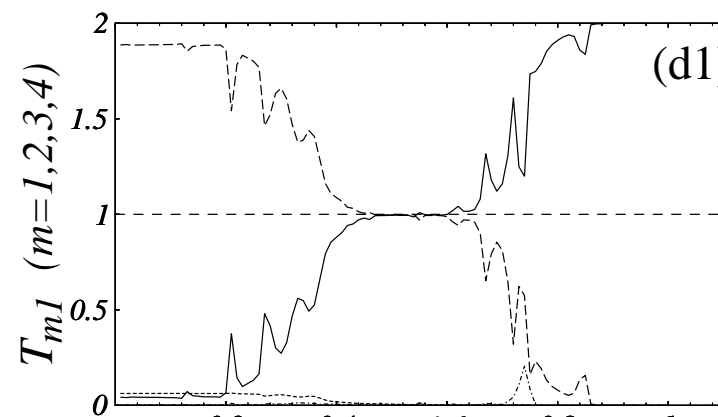
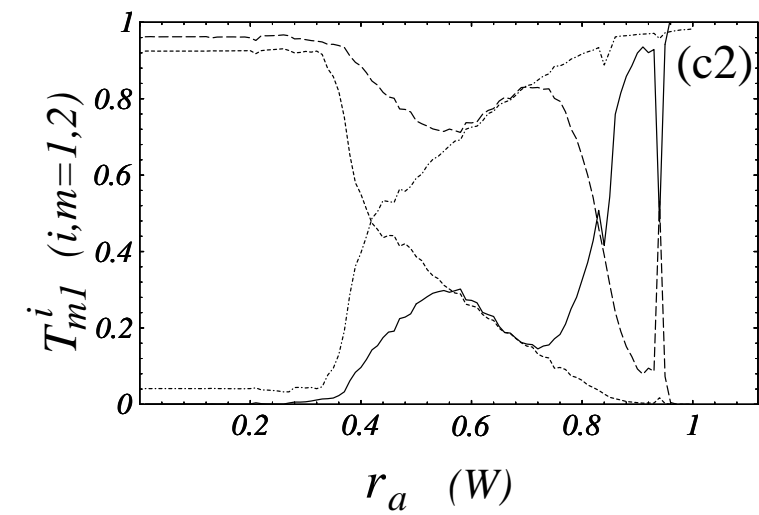
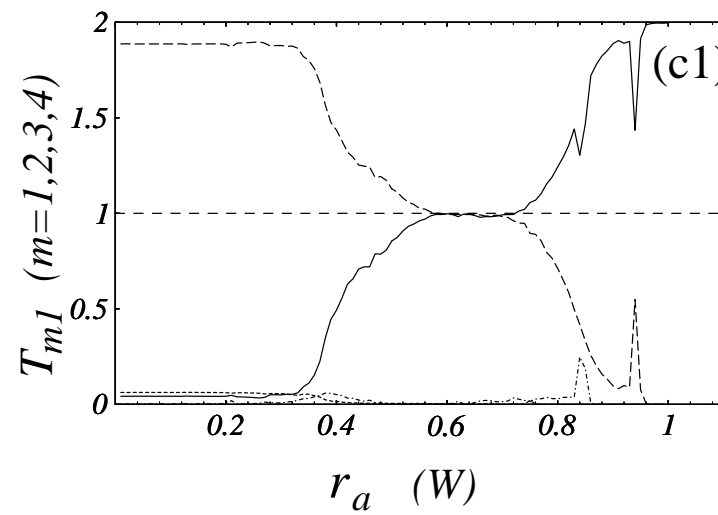
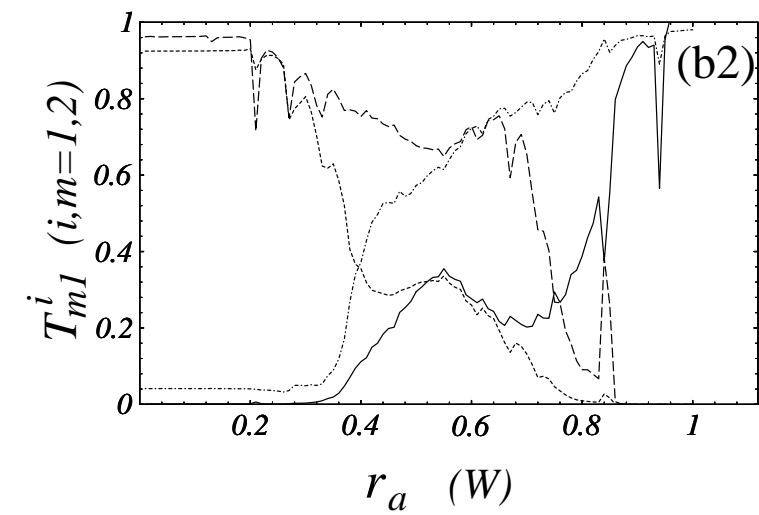
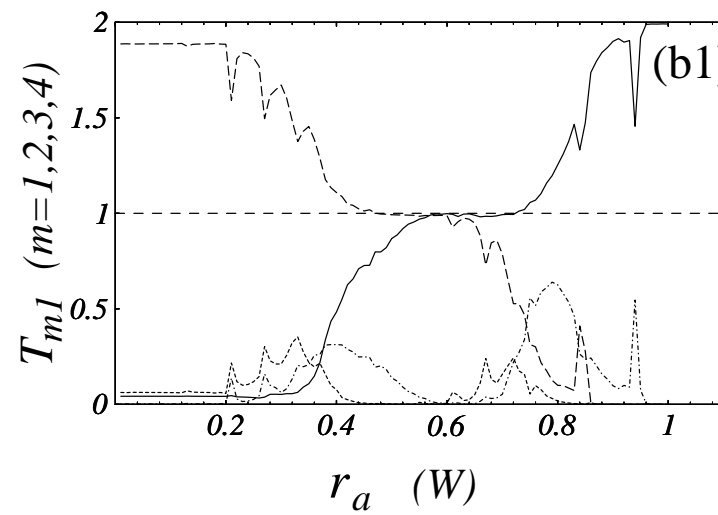
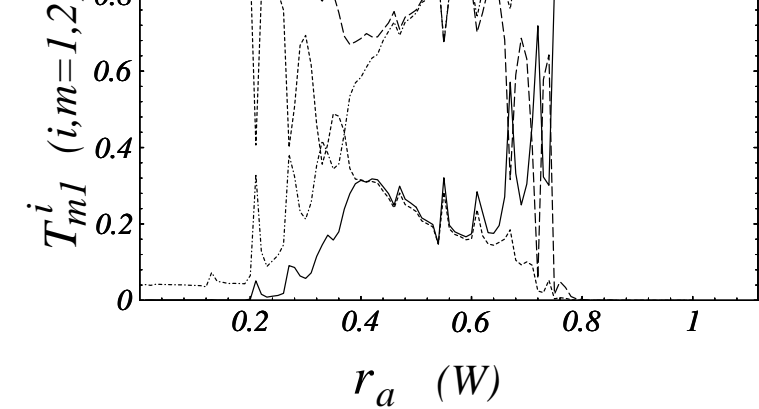
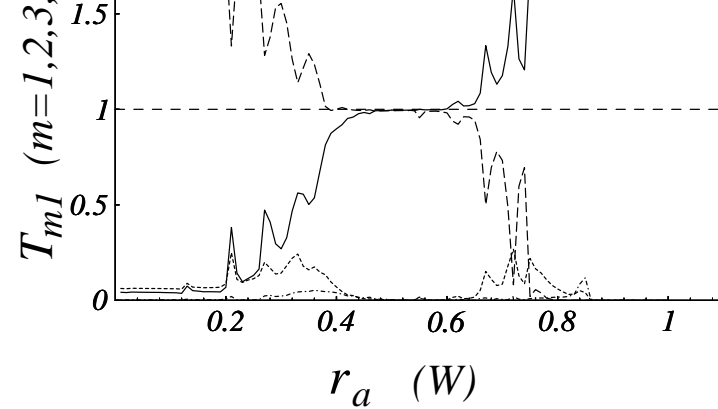


(c)



(d)

**Fig. 5**



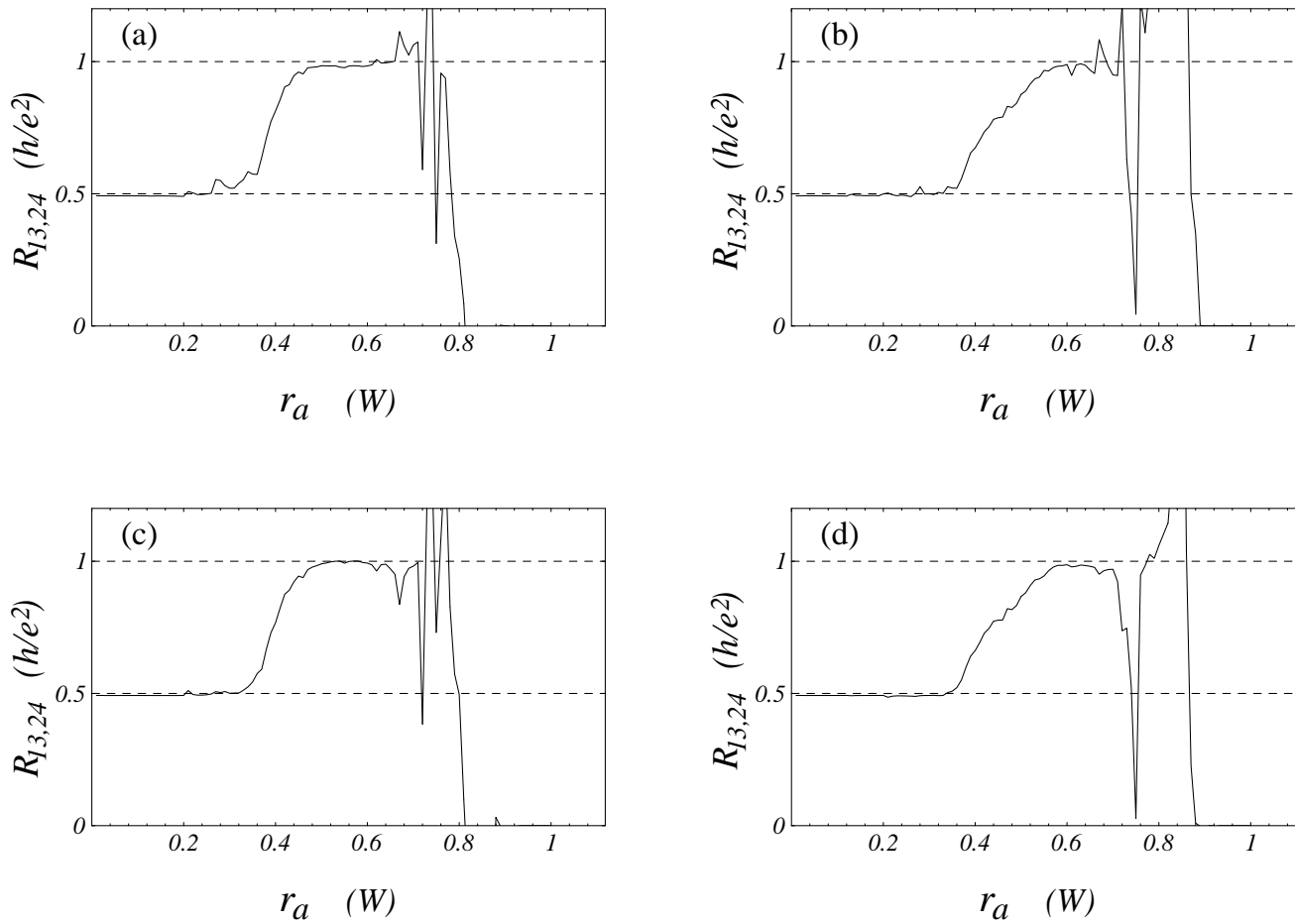


**Fig. 7**